The Cryosphere Discuss., 5, 1835–1886, 2011
www.the-cryosphere-discuss.net/5/1835/2011/
doi:10.5194/tcd-5-1835-2011

The Cryosphere Discussions

Laboratory study of frazil ice accumulation under wave conditions

S. De la Rosa[1,2] **and S. Maus**[1]

[1]Geophysical Institute, University of Bergen, Allégaten 70, 5007, Bergen, Norway
[2]Nansen Environmental and Remote Sensing Center/Mohn-Sverdrup Center, Thormøhlensgate 47, 5006, Bergen, Norway

Received: 27 May 2011 – Accepted: 13 June 2011 – Published: 8 July 2011

Correspondence to: S. De la Rosa (sara.delarosa@nersc.no)

Published by Copernicus Publications on behalf of the European Geosciences Union.

Abstract

Ice growth in turbulent seawater is often accompanied by the accumulation of frazil ice crystals at its surface. The thickness and volume fraction of this ice layer play an important role in shaping the gradual transition from a loose to a solid ice cover, however, observations are very sparse. Here we analyse an extensive set of observations of frazil ice, grown in two parallel tanks with controlled wave conditions and thermal forcing, focusing on the first one to two days of grease ice accumulation. The following unresolved issues are addressed: (i) at which volume fraction the frazil crystal rising process starts and how densely they accumulate at the surface, (ii) how the grease ice solid fraction evolves with time until solid ice starts to form and (iii) how do these conditions affect, and are affected by, waves and heat loss from the ice. We obtained estimates of the initial frazil ice solid fraction (0.04–0.05), the maximum solid fraction to which it accumulates (0.24–0.28), as well as the time-scale of packing, at which 95 % of the frazil reaches the maximum solid fraction (12–18 h). Comparison of ice thickness and wave observations also indicates that grease ice first begins to affect the wave field significantly when its thickness exceeds the initial wave amplitude. These results are relevant for modelling frazil ice accumulation and freeze-up of leads, polynyas and the seasonal ice zone.

1 Introduction

The growth of ice in open turbulent seawater is a regular process within a dynamic ice cover that undergoes frequent opening and closing, such as leads and polynyas. It is also produced in wintertime outside the ice cover – in the seasonal ice zone, which spans thousands of km^2 in both the Arctic and Antarctic. Under most conditions it starts by the nucleation of small crystals, called frazil ice. When wave- and current-generated turbulence is no longer capable of keeping the frazil ice in suspension within the water column, the crystals rise to the surface and accumulate in a layer of higher ice

TCD
5, 1835–1886, 2011

volume fraction. Agglomeration increases crystal interaction, which in turn implies an increased near-surface viscosity and damping of the oceanic turbulence. This positive feedback preconditions the freeze-up of the granular surface ice skim, often beginning in pancake-like patches of frazil ice referred to as shuga, then evolving to solid pancakes. Wadhams and Wilkinson (1999) present one of the few extensive ice sampling studies of the frazil/grease and pancake cover formed in the Odden ice tongue of the Greenland Sea, a region in the northern Polar Region known for extensive new ice formation in the presence of waves. The formation of such wave-induced frazil–pancake ice may become more recurrent in other Arctic regions, including the open water seasonal ice zone (Kinnard et al., 2008). This type of ice formation occurs on short time scales in highly dynamic turbulent ocean conditions and is very difficult to monitor. Even its basic properties such as thickness, salinity and solid fraction are still not well understood. Laboratory experiments provide an easily accessible and controlled environment to reproduce this type of ice growth and study in detail the physical processes that lead to the grease-pancake ice cover. There have been numerous laboratory studies on young ice growth, however, only a few consider frazil ice formation in a wave field and even less studies have taken place in water tank dimensions larger than a few meters. We highlight the studies of sea ice growing under turbulent conditions carried out by Martin and Kaufmann (1981), Wadhams (1988) and Newyear and Martin (1997). These studies showed that a grease ice layer dampens waves, with the wave amplitude declining exponentially with distance from the wave generator. They also indicate that the accumulation thickness of frazil ice crystals is limited by the energy flux from waves. However, a number of uncertainties remain regarding, for example, how the volume fraction, salinity and thickness of the grease ice evolve until the onset of pancake formation, and how these properties are related to observed wave conditions. More comprehensive laboratory experiments are clearly needed to resolve these uncertainties.

Wilkinson et al. (2009) briefly introduce a multidisciplinary study of laboratory grown frazil and pancake ice under turbulent conditions with a unique spatial and temporal

TCD
5, 1835–1886, 2011

resolution, compared to previous laboratory studies. The goals of the present paper are to give an overview of these experiments, present the extensive observations, describe the stage and evolution of a frazil ice field and to advance the understanding of frazil ice accumulation under wave conditions. The key uncertainties that we address include: (i) at which volume fraction the crystal rising process starts and how densely they accumulate at the surface, (ii) how this solid fraction evolves with time until solid ice starts to form, and (iii) how do these conditions affect – and are affected by – waves and heat loss from the ice.

The outline of this paper is as follows: Sect. 2 describes the experiment set-up and measurements made. Section 3 presents the observed spatial and temporal evolution of the measured properties: ice thickness, and salinity. Section 4 describes the derived properties, solid volume fraction and equivalent ice thickness. In Sect. 5, the temporal evolution is analysed and discussed with respect to overall ice growth driven by thermal forcing, and to the imposed wave field and its attenuation. We further analyse how the solid fraction and thickness change due to the transition from grease to solid pancakes and the mechanical redistribution by waves of known amplitude. Section 6 summarizes our main conclusions.

2 Experiment setup

Four ice-growth experiments carried out in two identically sized tanks under different wave scenarios are presented here. These are part of the Reduced ice Cover in the Arctic Ocean (RECARO) project that took place in two phases, during late 2007 and early 2008 at the Hamburg Ship Model Basin (Wilkinson et al., 2009). A schematic lay-out of each tank and instrument set-up is given in Fig. 1. The two tanks were separated by sealed wooden barriers and each was filled with NaCl water. The laboratory room temperature was maintained below freezing with cooling plates installed along the laboratory roof. A wave paddle at one end of each tank kept the water well mixed so that ice would form under turbulent wave conditions. Each of the four experiments consisted of

TCD
5, 1835–1886, 2011

two parallel runs with very similar conditions. Table 1 lists the basic physical conditions and ice growth characteristics for each experiment. E1 to E4 are the names given to each experiment; A and B are the names given to each tank (as labelled in Fig. 1). The same experiment/tank definition is used throughout this paper.

We aimed to start all experiments with completely ice-free conditions, but only E1 and E3 fulfilled this criterion. E2 and E4 were follow-up experiments for E1 and E3 respectively. Between subsequent experiment runs, the wave paddles were turned down and the tanks were cleared of ice. Removed ice from E1 was shuffled into a separate tank outside the cooling room, melted over night and reintroduced in liquid form into the tanks before E2. In the case of E4, the removed ice from E3 was not melted and refilled into the tank because of time constraints. Thus, some water was lost during these processes, reducing the water volume in the tanks for the two follow-up experiments: for E1 and E3 the water depth (H_w) was 0.85 m, for E2 it was 0.70 m and for E4 0.76 m. The experiment of longest duration and most regular sampling was E1 (see Table 1). All experiments nonetheless, included the full period of freezing from open water conditions until the formation of pancake ice and up to 30 h of frazil measurements are available for each.

A few pertinent results from these experiments have already been published. Wang and Shen (2010a) presented results for the end of E3 (not shown here), focusing on the wave attenuation and viscosity relation. (Note, their reference to tanks 2 and 3 in their paper, corresponds to tanks A and B here, respectively). In addition, De la Rosa et al. (2011) presented results from the latter half of E2, tank A, focusing on the thermodynamic and surface area cover changes during transition from a well-established frazil layer to pancake ice. (Note, hour 19 from E2 presented here corresponds to the start time 0 in their paper). Observations presented and analysed in this paper are primarily from loose, non-solidified frazil ice and to a less extent, shuga and pancake measurements.

TCD
5, 1835–1886, 2011

2.1 Air and water temperature and water salinity

Water electrolytic conductivity and temperature were continuously measured during experiments E1 and E2, with two Conductivity-Temperature-Depth (CTD) recorders (MicroCat SBE37-SM with 15 s sampling interval) placed stationary within the centre of each tank, at 0.20 and 0.45 m from the tank floor (hereafter referred to as bottom and top CTD's, respectively). No CTD measurements are available for E3. For E4, only one CTD was mounted in tank B (a SeaCat SBE19- SN 2161 profiler with a pump and sampling interval of 0.5 s). To convert the measured water conductivity to salinity we applied a conductivity ratio adjusted for NaCl water and calculated in gNaCl kg^{-1} units (as described in De la Rosa et al., 2011). The freezing temperature (T_f) was calculated using an approximation for NaCl solutions which gives −2.105 °C for water at 35 g kg^{-1} (see Maus, 2007). Table 1 lists the mean values for air temperature, water freezing temperature and the change in water temperature and salinity throughout the experiment. The water values are given for the top CTD closest to the growing ice cover.

Two thermistor chains of platinum resistance thermometer (Pico Pt-100) sensors were set up in the quiescent tank and covered air temperatures up to +16 cm above the surface. This tank was filled with NaCl solution to the same height as the other two tanks, and remained undisturbed from wave motion. The sensors were separated by 2 cm and measurement interval was 10 s. During E3 and E4 the two thermistor chains were located on the opposite end of the quiescent tank (crossed squares in Fig. 1), and air temperature was recorded at +8 cm above the surface.

2.2 Ice sampling

Ice thickness (H_i) was measured at fixed positions between 2 and 14 m along the tank (locations indicated in Fig. 1) and at approximately 1.5-h intervals. Measurements were made from two movable bridges placed across each tank. The ice sampling and thickness measurement procedure was adopted from earlier studies using a plastic

TCD
5, 1835–1886, 2011

cylinder (e.g., Wilkinson, 2005; Smedsrud and Skogseth, 2006). Uncertainties in these observations are of the order of ±0.3 cm (highest uncertainties are for the very first frazil crystals collected). At a subset of the sampling locations (refer to Fig. 1 legend), after measuring ice thickness, in-situ frazil ice samples were collected from the cylinder into a hand-held sieve to drain off the water before melting the ice in bottles at room temperature. The electrolytic conductivity of the melted samples was inferred from a hand-held conductimeter (WTW LP191, accurate to ±0.1 mS cm^{-1}). Sample weight and volume were obtained using a standard measuring scale (accurate to ±0.01 g) and a volumetric flask (accurate to ±0.1 ml), respectively. Shuga and pancake samples were also sporadically collected, photographed and their thickness measured. Size (surface diameter) was also measured in the along-tank direction and the across-tank direction. Pancake-like ice began to appear during the average times listed in Table 1.

2.3 Wave observations

To record the wave amplitude, two groups of underwater pressure transducers (Omega PX439-005) were placed at the central wall between the tanks. For E1 and E2, they were placed 60 cm from the tank floor and for E3 and E4 at 45 cm from the tank floor. Depth differences were corrected accordingly for each experiment, as described. Their positions are marked in Fig. 1, centred at 7.5 m and 11.5 m distance from the wave paddles (also see Wang and Shen, 2010a).

The wave frequency (f) for each experiment, obtained from the mechanical wave paddle reading, is listed in Table 1. During E1 the same frequency was applied in both tanks and maintained constant. During E2 a different frequency was applied in both tanks, yet also kept constant. The wave amplitude was decreased by ~2.5 cm during experiment hour 20. For the last two experiments, frequency was changed: during E3 three frequencies were applied, each of more than 5 h duration, with corresponding wave periods between 1.1 and 1.5 s. During E4 multiple wave changes were made between periods 0.9 to 2 s, each maintained for a minimum of 3 min up to 50 min. In laboratory studies, the tank size is a strong limitation, so lower wave frequencies

TCD
5, 1835–1886, 2011

could not be applied to get longer wave periods. However, the tanks used for the RECARO project were considerably larger than those used in other published wave studies (e.g. Martin and Kaufmann, 1981; Newyear and Martin, 1997).

3 Observations

3.1 Air and water temperature and water salinity

Figure 2a–d shows, for experiment E1, the time series of air temperature (T_a), the temperature difference ($T_w - T_f$) and the water temperature against salinity for both tanks. CTD data from the top and the bottom CTD's are shown in Fig. 2b–d. All temperature series show a similar behaviour and it appears that supercooling was absent from all experiments, at levels from 0.20 and 0.45 m from the tank bottom. There was some indication of slight supercooling at one of the four instruments when ice started forming (Fig. 2c, Tank B), but this signal is weak (0.01 K). During the first 5 h of E1, temperature decreased further by ≈0.1 °C in the water and by 3.5 °C in the air, yet ice formation had already begun (the first ice thickness measurement was made a half hour after the beginning of this time series). During experiment 9 h of E1, a wave paddle stop occurred for 2 h, due to a mechanical problem in both tanks. This caused a warming of the tank water (Fig. 2b and c). Water temperatures decreased again once the wave paddles were restarted an hour later, accompanied by a rise in the air temperature (Fig. 2a). During the first 5–10 h of E2 (not shown), a salinity decrease was measured in Tank B while salinity increased in Tank A, the stratification dissipated due to wave stirring after 2 h. This could be an indicator that an exchange took place between the tanks and that the isolation between the tanks was not perfect. The tank differences could have also been caused by the melt water refill before the start of E2. The measurement record for E4 (also not shown) started around 2.4 h after the actual experiment began.

TCD
5, 1835–1886, 2011

3.2 Heat flux from surface

The bulk heat flux through the tank water surface (with or without ice cover) is, for a perfectly insulated tank and neglecting mass loss by evaporation, approximated as:

$$Q = H_w C_{pw} \rho_w \left(-\frac{dT_w}{dt} \right) + \frac{dH_e}{dt} L_f \rho_i = Q_s + Q_i (\mathrm{W\,m^{-2}}) \quad (1)$$

The heat flux due to cooling (Q_s) during the first 10.5 h of initial cooling when ice formation was absent, is given by the first term to the right: obtained from the rate of change in water temperatures, T_w, measured from the top and bottom CTDs, the water depth, H_w, the specific heat capacity of water, $C_{pw} = 4020.6\,\mathrm{J\,kg^{-1}\,K^{-1}}$, and the water density, $\rho_w = 1027$ ($\mathrm{kg\,m^{-3}}$). The period of cooling was defined as the time when $T_w >= -1.5^{\circ}\mathrm{C}$.

The heat flux during frazil ice growth Q_i is given by the second term: the latent heat of fusion, L_f=330.7 $\mathrm{kJ\,kg^{-1}}$ (valid for a 33.3 $\mathrm{g\,kg^{-1}}$ NaCl solution at $-2.0\,^{\circ}\mathrm{C}$), the pure ice density; $\rho_i = 917\,\mathrm{kg\,m^{-3}}$ and the change in equivalent ice thickness, defined as $H_e = \overline{H_i v_s}$, where v_s is the solid volume of ice.

The mean Q_s obtained from water temperature differences from the top and bottom CTDs during the initial cooling period, was $81.6 \pm 8.6\,\mathrm{W m^{-2}}$ for tank A and $81.5 \pm 2.8\,\mathrm{W m^{-2}}$ for tank B. We should note that the variability of Q_s obtained from the two CTD sensors in each tank, was very similar, yet, a notably larger (about 20 % higher) variability is observed in tank A than B. We take this as an indicator that the apparent heat flux variability is not related to the heating intervals from the roof cooling plates, but rather to the variability of the water movement itself (e.g. wave-generated residual currents advecting temperature anomalies past the CTD sensors). In Sect. 4.1 we determine the total heat flux after the freezing point is reached (Q_i), based on ice growth observations for each experiment.

TCD
5, 1835–1886, 2011

3.3 Ice thickness

Figure 3 shows how the measured ice thickness varied along the tanks and in time (indicated by the exponentially modelled thickness distribution lines at 5, 15 and 25 h, where available). We see that the along-tank ice thickness distribution becomes approximately uniform with time, for all experiments in tank A, and experiments E2, E3 and E4 in tank B. This occurred earlier for E2 and E4, which began with an ice thickness of 3.5 cm and 3 cm respectively in tank A, and 2.8 cm and 4.2 cm, respectively, in tank B. Ice accumulation at the end of the tanks only noticeably occurred during experiments E1 and E3 after 5 h of freezing. However, for the last three experiments, the along-tank distribution of ice thickness became almost homogeneous. For E2 and E4 this happened after just 5 to 8 h of ice growth. These two experiments may be regarded as two special cases where ice formation had started several hours prior to the first sampling.

We attempted to reproduce the measured ice thickness distribution (in space and time) of the four experiments using two model functions:

1. a power law approach $H_i = h_1(x)^{a_1}$, and
2. an exponential growth function $H_i = h_2(1 - \exp^{(-a_2 x)})$

The mean modelled increase, H_{im}, was obtained by integrating in each case the measured ice thicknesses over the tank length before the beach (16 m) from x1 = 0 to x2 = 16. The residuals from the difference between predicted and measured ice thickness obtained by each method, rendered a significantly lower (on average 3 times lower) mean standard deviation ($\pm 1\overline{\sigma}$) for the exponential fit (0.49 cm as opposed to 1.25 cm). In addition, the coefficient a_1 from the power law relation varied with time and also rendered some negative values.

We thus use the exponential expression h_2 to fit ice thickness along the tank length (see lines for 5, 15 and 25 h given in Fig. 3). Figure 4 compares the mean of the measured thicknesses with the mean fits ($\overline{H}_{im}$) obtained from the exponential relation.

TCD
5, 1835–1886, 2011

The means of the measured values are overall minimally higher than those obtained from the exponential relation, likely because the integration extrapolates towards high values at tank locations (14.5 to 16 m) where no measurements were done.

3.4 Frazil ice solid fraction

From the measured ice salinity with unknown brine content (variable due to the sampling/drainage protocol, as discussed in De la Rosa et al., 2011), we may estimate the volume fraction of ice as:

$$v_s = \frac{M_m}{V_g \rho_i} \left(1 - \frac{S_{im}}{S_b}\right), \quad (2)$$

where V_g is the measured grease/frazil ice volume before drainage, M_m and S_{im} the mass and drained salinity of the collected samples after sieving and melting and S_b the brine salinity. Details on the derivation and application of Eq. (2) are further shown in Maus and De la Rosa (2011). Resulting v_s values are presented in Sect. 4.

The volume fraction of pancakes cannot be properly determined with this method, as pancakes were broken during sampling, so the exact volume of the sampled pancake pieces before melting, was unknown. For reference, Wang et al. (2008) found large uncertainties when applying this approach for calculating pancake ice volume fractions. In our method, the main uncertainty in the determined solid fraction comes from the uncertainty in frazil thickness (±0.3 cm) read from the sampler, from which V_g is computed. This implies maximum errors of 0.05 in the beginning of the experiment when ice thickness is small. Typical errors however decrease from 0.02–0.03 after a few hours to values close to 0.01 for most of the time.

TCD
5, 1835–1886, 2011

3.5 Frazil ice salinity

Ice salinities were calculated based on the frazil ice solid volume fraction (thus, correcting for the unknown loss of brine that occurs during frazil ice sampling), using:

$$S_i = \frac{S_b}{1 - \frac{\rho_i}{\rho_b}\left(1 - \frac{1}{(1-v_s)}\right)}, \quad (3)$$

(obtained from mass and salt conservation, Maus, 2007; Maus and De la Rosa, 2011). The brine salinity was not directly measured, so we assume $S_b = S_w$. The brine density in the ice was approximated as ρ_b=1000+(0.77*S_b). As ice salinity values depend on the drainage protocol we do not present the sieved sample salinities, S_{im}, but just mention that they are on average 7 g kg^{-1} (and up to 40 %) smaller than the actual in situ undrained salinities (addressed further in Maus and De la Rosa, 2011).

For experiments E3 and E4 no CTD measurements were available at the beginning of the tests. In E4, tank B, observations started 2.4 h after the beginning of the experiment. We thus obtained S_w for the initial period from the heat loss Q_s via S_{wo}, the initial water salinity before ice formation, required for estimating ice production and the change in S_w, by iteration in time as:

$$S_{w(t)} = -\frac{Q_s}{L_f \rho_i}\frac{S_{w(t)}\Delta t}{H_w} + S_{w(t+1)}, \quad (4)$$

where Δt is the timestep between the salinity measurements, obtained from the mass and salt balance (e.g., Eq. 6 in De la Rosa et al., 2011). The higher initial salinity S_{wo} for E4 (~35.4 as given in Table 1) may be explained by the removal of ice from E3. For E3 the exact initial salinity is not known, but the target value when filling the tank was as for E1. Hence, the value of S_{wo} of 33 was used in Eq. (3).

TCD
5, 1835–1886, 2011

Once S_i was calculated, the mean frazil ice salinity was determined summing all measurements along the tank at any time instant as:

$$\overline{S}_i = \frac{\sum S_i H_i}{\sum H_i} \quad (5)$$

The other ice properties presented later on (v_s and H_e) were also computed using this averaging method. Table 1 lists the maximum and minimum ice salinity that was measured in each experiment and tank. Also here, the main uncertainty in the determined salinity comes from the reading error in frazil thickness (±0.3 cm). This creates a relative uncertainty of $\sim dH_i/H_i$ with a maximum of 2 g kg^{-1} at the beginning of the experiment when ice thickness is small. Typical systematic errors however decrease from initially 0.5–1 g kg^{-1} during the first hours to 0.3–0.5 g kg^{-1}.

4 Results

The mean ice salinity values obtained from Eq. (5) for all experiments are shown in Fig. 5a, b. Note that all salinities in E4 that started with a 2 g kg^{-1} higher salinity, are shown normalised by 33/35.38. The scatter (sampling variability) is large, but in general the experiments show a decrease from initial values above 30 g kg^{-1} to final values around 25 g kg^{-1}. For E2 and E4, a salinity increase is apparent, yet this may be attributed to the low number of samples (increasing variability) and the higher sampling uncertainty during low ice presence (i.e. the first 7 h of freezing). Figure 5c, d shows the mean values obtained also from Eq. (5), but applied to v_s values instead of S_i. A general increase from 0.07 to 0.30 is observed in experiments E1 and E3, whereas the other two experiments present less clarity due to the reasons already mentioned.

Looking at the S_i and v_s histogram distributions of all frazil data (Fig. 6a, b, respectively), we distinguish two main modal peaks, which appear to correspond to (1) the start (first 8 h) of frazil conditions ($v_s \approx 0.08$ to 0.12 and $S_i \approx 29$ to 31 g kg^{-1}) and (2) to the pre-pancake formation transition ($v_s \approx 0.18$ to 0.26 and $S_i \approx 26$ to 28 g kg^{-1}). Scrutiny of the time series (Fig. 5) confirms this interpretation.

TCD
5, 1835–1886, 2011

If we further consider separating the two experiments that start with ice-free conditions (E1 and E3), from those that do not meet this criteria (E2 and E4), we observe considerably different distributions. The first group (not shown) presents two peaks in v_s at 0.11 and 0.19 and corresponding peaks in S_i at ~30 and 27 g kg^{-1}. The second group (light shades within Fig. 6), presents a single modal peak spanning from $v_s = 0.22$ to 0.24 and at $S_i = 26$ to 28 g kg^{-1}, indicating that this ice is at a slightly older aging stage. We will analyse this in more detail in Sect. 4.3. First, we want to show if we measure any change in heat flux during ice growth Sect. 4.1 and how the wave field is affected, once frazil ice accumulates to its maximum thickness Sect. 4.2.

4.1 Equivalent ice thickness

For the freezing period, the heat flux for each experiment may be obtained from a fit of the equivalent ice thickness against time, ($\overline{H_e} = H_{e0} + q_h t$), which we apply up for the periods when mostly frazil ice was present (t <25 h for E1 to E3 and t <6 h for E4). From, the fitted coefficient q_h one then obtains the heat flux for each experiment as $Q_i = q_h L_f \rho_i$.

Figure 7a, b show the observed mean $\overline{H_e}$ and corresponding linear fits to obtain Q_i. For E2 and E4 the presence of ice at beginning of the experiments is clearly seen (with initial values of 0.4 to 0.7 cm respectively), yet the linear slopes defining the ice growth rate run almost parallel to those of E1 and E3.

The confidence for the $\overline{H_e}$ growth line intercepts (H_{e0}) seen in Fig. 7a, b is lowest for E3, where the intercepts are negative and also for E4, where the fits are based on just four measurements. We may consider the difference between the mean water and air temperatures as an indicator of the possible changes observed in Q_i, derived from the procedure explained above, we see a small decrease in Q_i. Figure 8 shows the Q_i values for each experiment and tank, with their corresponding upper and lower 95 % confidence interval limits against the temperature difference. The derived heat flux for all experiments in tank B, is lower than the constant Q_s ~82 Wm^{-2} that was initially found during the cooling phase.

TCD
5, 1835–1886, 2011

In laboratory conditions, with relatively constant air ventilation and radiation, the heat flux leading to ice growth may be approximated by the empirical growth law $Q = k_a(T_a - T_s)$, where T_a is the air temperature at a fixed reference level above the ice, and T_s the ice or water surface temperature. For the cooling period, which gives Q with highest significance, we estimated the water-atmosphere heat transfer coefficient $k_a = 8.8\,\mathrm{W\,m^{-2}\,K^{-1}}$, with T_a from the +8 cm thermistor. In Fig. 8 we plot the linear growth law mentioned above through the data for all experiments. The line runs reasonably well through the experiments that have lowest uncertainty for Q (i.e. the cooling period, tanks A and B, E1 A and B as well as E2 A), supporting the applicability of the growth law. It is notable that E3 falls above the linear relation while E4 falls below, indicating a reduced heat flux in a stage of higher pancake coverage (E4 compared to E3).

4.2 Wave height and ice thickness

We know that waves force the grease ice towards the opposite end of the wave tank as the result of the induced wave drift and the radiation stress exerted by the wave field (Martin and Kauffman, 1981). Yet, we want to understand why/how the growing (frazil) ice is initially distributed unevenly along the tank (accumulating furthest away from the wave paddle), but in the final stage it ends up being quite evenly distributed (as seen in Fig. 3). From the wave amplitude, A, at two locations in the tank separated by $\partial_x = 4$ m (taking the central location at each sensor group), we compute the attenuation rate, q, of the waves between the two measured locations, similarly to Wadhams (1988) or Newyear and Martin (1997):

$$A_x = A_0 \exp^{-q\partial_x}, \tag{6}$$

We use the mean wave amplitude of each sensor group to reduce noise caused by the individual sensors. Here we attempt to illustrate the interaction of three parameters: the spatial attenuation rate q, the wave height w_h and the ice thickness. To do so we normalise the wave height and the ice thickness by the initial (open water) wave height

TCD
5, 1835–1886, 2011

(i.e. twice the initial wave amplitude A_0 listed in Table 1; w_{h0}). The mean ice thickness and mean amplitude data at the two wave sensor group locations were used, as the same variability was observed in the time series at both locations. Figure 9a shows for E1 w_h against the normalized ice thickness, H_i/w_{h0}. It is clearly observed that at the start while frazil is still thin, w_h remains constant in both tanks. A small increase occurs after the wave paddles restarted (there was a wave stop between 9 and 11 h) and w_h begins to decay sharply once $H_i > 0.9 w_{h0}$ in tank A, or $H_i > 0.7 w_{h0}$ in tank B. During E2 a sudden reduction in wave height to half its size was induced during experiment 20 h (10 cm to 5 cm in Tank A and from 13 to 8 cm in tank B). To avoid misinterpretation, this experiment was not shown together with E1 in Fig. 9a. Figure 9b shows the evolution of the spatial attenuation rate with H_i/w_{h0}, for experiments E1 and E2. It is observed that q begins to increase above the noise level as $H_i > 0.5$–$0.6 w_{h0}$. Above $H_i > 0.7$–$0.9 w_{h0}$ there is a considerably increase in the wave attenuation.

It is known that wave reflections vary with ice thickness and other parameters – for more details see Wang and Shen (2010a, b). Yet, the length (L) of the tank is its natural scale of damping and resonance. Interpreting it in terms of the attenuation rate q, 1/L may be thought as a forced e-folding scale. Here this is plotted in Fig. 9b as a continuous dashed line to indicate the level below which the estimated q may be interpreted as noise. In both experiments, the values for Tank A (diamonds) appear to lie mostly below the 1/L reflection scale of the tank. During the first 5 h of E1 A, negative q values were obtained (removed from Fig. 9b), an indication that too little ice was present and internal reflections took place. In Fig. 9c we illustrate the observations by normalising q by the apparent average noise level from the two tanks. We see that in both tanks, q begins to rise considerably above the apparent noise level when H_i/w_{h0} becomes larger than 0.5–0.6, with a strong increase in the range 0.7–0.9.

The wave data for E3 (not shown) did not resolve any response of attenuation rate and wave height with the normalized ice thickness growth, since only three data patches were visible, corresponding to the times the wave frequency was changed. For E4 (also not shown), the data values are scattered, yet high q values already occur

TCD
5, 1835–1886, 2011

after experiment 2 h. The experiment was also characterized by a solid pancake layer already forming after just 6 h of freezing, and in contrast with E2, the ice cover evolved into a solid layer and showed no gaps between pancakes.

The histogram distribution of H_i/w_{h0}, Fig. 10, confirms that the normalized ice thickness is limited by the wave height and thus, constrained to values not much larger than 1.5. When a normalized ice thickness of ~1.5 to 1.7 is reached, the along-tank distribution for E1 to E3 appears to flatten out to become more- or- less even. However, from histograms distributions grouped in time (not shown), it is clear that the grease ice thickness for E1 to E3 was still increasing and had not reached a limiting value. Only in E4 were H_i/w_{h0} values close to 3 reached, before the ice started to consolidate.

We find for E1 to E3, that the ice first surpasses the ice thickness to wave height ratio of equality ($H_i/w_{h0} > 1$) at the end of the tank, after about 12 h of freezing (not shown). As freezing continues, the maximum ice thickness extends towards locations nearer to the wave paddle.

4.3 Frazil ice compaction rate

Now that we know how heat flux and the wave properties change with the growing ice cover, we want to define what the ice properties are at the time initiation of pancake formation begins. We evaluate the data in terms of a simple packing law, where we assume that the rate by which the solid fraction approaches a maximum value v_{smax} is given by $d(v_{smax} - v_s)/dt \approx c_1(v_{smax} - v_s)$ for $v_s < v_{smax}$. Making this assumption leads to the following an exponential growth relation:

$$\overline{v_{s(t)}} = v_{smax} - (v_{smax} - v_{s0}) \exp^{\left(-\frac{t}{t_c}\right)} \quad (7)$$

The latter equation describes the evolution of the average solid fraction of a fixed grease cover with time. However, it does not consider the aspect that new frazil continuously accumulates on the underside of the existing grease layer. To approximate this process we make a second approach, $d(v_{smax} - v_s(z_e))/dz \approx c_2(v_{smax} - v_s(z_e))$, where

TCD
5, 1835–1886, 2011

z_e is the cumulative equivalent thickness measured upwards from the lower grease ice boundary. We then integrate this last equation from the ice-water boundary to the top z_e, and obtain a solution for the local solid fraction at the surface of ice of thickness H_e=z_e:

$$v_{s(z_e)} = v_{smax} - (v_{smax} - v_{s0}) \exp^{\left(-\frac{z_e}{H_c}\right)} \quad (8)$$

Integration of Eq. (8) from $z = 0$ at the ice-water interface to $z = z_e = H_e$ gives the average solid fraction:

$$\overline{v_{s(H_e)}} = v_{smax} - \left(\frac{H_c(v_{smax} - v_{s0})}{H_e}\right)\left(1 - \exp^{-\frac{H_e}{H_c}}\right). \quad (9)$$

Values $v_s > 0.30$ were not included in the analysis, as they were identified as frazil samples that had begun to freeze internally. From the range of coefficients obtained, we built the sum of square residuals and selected the one that gave the lowest value (highest correlation) to define v_{smax}. The initial v_{s0} of the data was then estimated, given as $v_{s0} = v_{smax} - c_1$ for the time relation and $v_{s0} = v_{smax} - c_2$ for H_e.

We may interpret the coefficients in the exponential packing equation as typical decay time and/or thickness scales, at which t=1/c_1(or H_e=1/c_2) ≈63 % of the maximum packing is achieved. Figure 11a and b shows the maximum (dashed curve) and mean (solid curve) v_s exponential relations with H_e for all the experiment data and E1 alone, respectively. A v_{s0} of 0.04 and 0.03 is obtained, respectively and a v_{smax} of 0.28 and 0.24. These values represent the maximum v_s values, analogous to the most compact frazil found at the ice skim surface. The estimated equivalent ice thickness reached once 95 % of the packing has taken place is 0.99 cm for all data and 0.42 cm for E1. For the v_s-time fit (Fig. 11c), we obtain $v_{s0} = 0.04$, $v_{smax} = 0.23$ and a packing time scale of about 6 h. The vertical dashed-black line in Fig. 6c indicates this estimated time-scale. Considering the natural variability of the data, the maximum value, below which the majority of observations fall was found to be $v_{smax} \approx 0.28 \pm 0.02$. This is a slightly higher estimate than that mentioned in De la Rosa et al., 2011 (where frazil v_{smax} was estimated as 0.266 ± 0.026), yet within the variability range.

TCD
5, 1835–1886, 2011

4.4 Pancake

The approximate start time of pancake-like ice formation is given in Table 1. Thickness and diameter observations were made for sporadically sampled pancakes in each tank after these times. Diameter measurements were subdivided according to size into shuga (<= 5 cm) and medium sized pancakes (> 5 cm). Very few observations (<15) were made during E1 and E2, so these are not considered representative for the full tanks. The mean shuga diameter observed during all experiments (estimated from 106 observations) was 1.5 to 2.0 ± 1.0 cm. The average medium sized pancakes measured during E3 were 15 ± 9 cm, those measured during E4 were 21 ± 12 cm (estimated from 25 and 80 observations respectively).

If we consider the distribution of sizes along the tank (not shown), during E3, medium sized pancakes were observed only after 9 h of experiment start and were more abundant between 8 m to 14 m away from wave paddle. On the other hand, during E4, the along-tank pancake size distribution was much less defined. Medium sized pancakes were observed everywhere along the tank, from already 6 h into the experiment. A comparison of the pancake thickness (H_{ipk}) with frazil thickness H_i from E4 and E5, indicated that on average, the maximum pancake thickness was lower than the average frazil thickness. An approximate relation of maximum pancake thickness $H_{ipk} = H_i/1.5$ is determined from these observations.

5 Summary and discussion

We have presented results from a laboratory study on the growth of frazil ice under the presence of waves. Our main focus was to monitor the properties of frazil ice, i.e. its salinity, solid ice volume fraction and thickness, as they evolve with time. To do so we measured these properties with temporal resolution of a few hours and at 7 evenly spaced positions horizontally along the tank. Supplementary observations to interpret the ice cover evolution include (i) water conductivity/salinity and temperature monitored near the tank's centre, (ii) the wave amplitude and its decay, as well as (iii) air temperatures at different vertical levels above the ice/water surface. While the same laboratory

TCD
5, 1835–1886, 2011

facility has been used earlier to study frazil ice growth in a similar setup (Wilkinson, 2005), the present observations constitute, in terms of temporal and spatial resolution, a unique dataset of frazil ice observations under controlled growth conditions. In addition, we have introduced a number of practical and theoretical improvements on earlier work.

All experiments proceeded under very similar heat flux forcing, in principle in the following way: Once the freezing point was reached, frazil began to form over the whole surface of the tank but was accumulated at the "down-wave" end of the tank, presumably due to wave-induced Stokes drift. The corresponding frazil thickness profiles along the tank after a few hours became almost linear. Once the "down-wave" thickness approached one to two times the wave amplitude, it did not appear to increase much further, yet from then on a wedge propagated "up-wave", soon filling up the tank with a similar ice thickness. In most experiments the further increase in thickness remained rather uniform over the tank, i.e. there were little horizontal thickness gradients, once the latter had reached the same value as the wave height. Pancake formation was observed at different times for two experiment groups (after 17–21 h for E1 and E2 compared to 3–5 h for E3 and E4), nevertheless, most of the frazil observations stem from the periods without pancakes. The following discussion thus refers mainly to the state of frazil ice in the absence of pancakes.

It is recalled that Experiments E1 and E3 started from similar conditions, with ice formation commencing after an initial cooling period when the water had reached its freezing point. Experiments E2 and E4 did not initiate from a cooling phase and presented a rather rapid appearance of a significant amount (~ 4 cm) of ice in both tanks, suggesting that ice crystals must have been present at the start of both these experiments. None of the CTD instruments indicated considerable supercooling, with upper CTD temperatures in tank B just reaching 0.01 K below freezing during the beginning of the experiment, between hours 6 to 7. However, this does not mean that the frazil grew without supercooling. The upper instrument, at which slightly lower temperatures were measured, was still 40 cm from the surface, while wave heights were typically less than

TCD
5, 1835–1886, 2011

10 cm. As the strongest downward mixing of surface cooling can be expected on a length scale of the waves, there might have been supercooling near the surface. For example, Smedsrud (2000) showed temperature profiles, with 0.04–0.06 lower temperatures near the surface of this tank. We also see, in one of the tanks, a 0.02–0.03 K higher bottom temperature, but do not have profile information. The presence of such a gradient would thus be consistent with a slight supercooling of a few hundredths of a degree, as reported for studies with similar moderate heat fluxes (e.g. Carstens, 1966; Osterkamp et al., 1983; Clark and Doering, 2009).

5.1 Salinity

Frazil salinities are found to decrease, over the course of one day, from average values slightly above 30 to values close to 25. This result is very robust, not only for both E1 runs, but also for the other experiments. The only exceptions of initial lower salinities were found in E2, which started already with an equivalent ice thickness of 0.7 cm, and E4 (if corrected for the 2 units higher water salinity that characterizes this experiment). Referring back to the discussion above, the lower salinities could be explained by the existence of some old frazil ice, from the end of E1 and E3, at the beginning of the follow-up runs E2 and E4.

Our approach to present ice salinities as in situ values is different from what most authors have presented in previous work. In most studies the authors have drained and sieved the frazil, as we did, yet interpreted this residual salinity in terms of the potential entrapment of frazil ice, without recomputing the intrinsic salinity from the solid fraction. We think that the approach of using sieved or drained salinities alone is of limited value due to the following reasons: Firstly, the drainage protocol is subjective, as factors such as time and intensity of shaking, temperature and cohesion of frazil at sampling, temperature in air and of sieve are hardly reproducible from study to study. Secondly, the salt adhering to the crystals during sampling is likely not representative for the salt at a later stage, with higher solid fraction. E.g., if the salt depends on the specific surface of crystals, the latter will decrease simply by their coarsening.

TCD
5, 1835–1886, 2011

However, we report here on some previous observations. (Note: ice and water salinity units are given in this discussion as mentioned within the referenced publications). First, Martin and Kauffmann (1981) reported that 31 % of the salt from a 38.4 g kg^{-1} NaCl solution remained in the frazil. For their solution this corresponded to 11.8 ± 2.1 g kg^{-1}, while, after scaling for standard seawater[1] (35 psu), this corresponds to a frazil salinity of 10.9. Doble (2007) reported drained frazil salinities in the Weddell Sea between 8 and 19 psu. His values decreased from the outer ice edge (14 to 19 psu), via the middle and inner ice zone (10 to 15 psu) to long scale distance (8 to 12 psu). Wadhams and Wilkinson (1999) reported, for frazil and slush collected between pancakes in the Greenland Sea, even a larger range of 5 to 22 psu. Smedsrud (2001) noted salinities of sieved slush in the range 20 to 28 (water salinity 36 psu), while Smedsrud and Skogseth (2006) reported on values in the range 16 to 28 (water salinity 33 to 35 psu). Also Reimnitz et al. (1993), used a similar method to derive apparent salinities of drained frazil from 12 to 20 (at water salinity of 32 psu). We note that our drained salinities (not shown in the present study) lie within the range 14 to 26 g kg^{-1}, similar to those obtained by Wilkinson (2005) in the Greenland Odden during 2002, (17 to 24 psu) and the above mentioned values by Smedsrud and Skogseth (2006) from observations in the Storfjorden polynya, Svalbard. Therefore, even when only considering very young frazil, sieved frazil salinities vary in a range 10 to 30 g kg^{-1}, far from the intrinsic range 25 to 32 g kg^{-1} presented here. While our highest values appear large, also Onstott et al. (1998) reported an initial salinity of 29 for thin grease ice growing from a water salinity of 30 psu. As pointed out in De la Rosa et al. (2011), proper modelling of salt fluxes requires the intrinsic, not the drained salinity. Finally, while the salinity of sieved and drained frazil samples alone is not an objective frazil property, we point out that the combination of sieved and true salinities may indeed provide insights into frazil morphology, as discussed for our data in a follow-up paper (Maus and De la Rosa, 2011).

[1] per definition a seawater salinity of 35 psu corresponds to a salinity of 35×1.005 g kg^{-1}

TCD
5, 1835–1886, 2011

5.2 Solid volume fraction

The solid volume fraction and ice salinity are related to each other by Eq. (2) and (3). For young frazil, when the brine salinity is close to the seawater value, the volume fraction v_s is thus proportional to $(1 - S_i/S_w)$ and increases with decreasing ice salinity. The time-sequence of average volume fractions (Fig. 5c, d) shows an increase from low initial values of 0.05 to 0.3 over the course of one day. Corresponding to the low salinities, initial values are exceptionally high for E2 and E4, and interpreted as older frazil ice already present at the beginning of these runs.

To analyze the increase in solid fraction due to packing we have considered the relation $d(v_{smax} - v_s)/dt \approx c_1(v_{smax} - v_s)$. This gives an exponential equation (Eq. 8) for the solid fraction that may be fitted by least squares to obtain the initial solid fraction v_{s0} at the onset of ice formation, a maximum solid fraction v_{smax}, and the time constant c_1, indicating that after time $1/c_1$ 63 % of the packing has taken place. The time dependence was determined for E1 with high temporal resolution (Fig. 11c) and the same fit was applied to the equivalent ice thickness data using all experiment runs (Fig. 11a), each of which had a different initial ice thickness. We obtained $v_{s0} \approx 0.04$ for both approaches, $0.23 < v_{smax} < 0.28$, as well as a decay time $1/1c_1 \approx 6$ h from the time-exponential fit. The corresponding equivalent thickness decay scale was $1/1c_2 = 0.14$ cm for E1 and $1/1c_2 = 0.33$ cm when all experiments are fitted. With a constant heat flux, thickness and time, this should be proportional to $Q/(L_f \rho_s)$, and we may convert $1/c_2$ to a decay timescale of 1.7 h for E1 and 4.0 h for all data. While the fit against time yields an average response from all tank locations, it does not account for advection and redistribution; i.e., as long ice accumulates strongly at the end of the tank, most of the remaining tank area has ice that is younger than the average age of ice, yielding a larger time constant. It is the fit against the equivalent thickness that sorts the ice samples most reliably according to their age, being less biased by advection. Furthermore, it may be argued to be physically consistent with the mechanism of packing by loading (equivalent ice mass and buoyancy). That the E1 estimate (0.14 cm) for the decay

TCD
5, 1835–1886, 2011

thickness scale is lower, may have to do with the shutdown of the wavemaker from 9–11 h in this experiment. The decay scale based on all data, 0.4 cm, implies that 95 % packing is reached after 1.2 cm of equivalent ice growth. In a parallel paper (Maus and De la Rosa, 2011) we discuss further that this scale is consistent with other laboratory studies.

To interpret these values we need to note that the change in solid fraction, as we have monitored it, does not only resemble the packing of existing ice. It results from three processes: (i) packing of existing frazil, (ii) growth and coarsening of existing crystals and (iii) secondary nucleation of new crystals. It is clear that processes (ii) and (iii) are related to ice growth due to the ongoing heat loss. However, these two thermodynamic processes will counteract each other. On the one hand (ii) may be thought to take place within the existing surface grease, thus increasing the solid fraction by growth of crystals. On the other hand (iii) will decrease the solid fraction, at least on the order of the wave height, if nucleation of crystals takes place within the water column, followed by settling of new crystals as high porosity frazil at the bottom. We obtained a simple solution to this problem by integrating Eq. (7) to obtain the average solid fraction, assuming that the local solid fraction is a function of the accumulated frazil mass below it. For a validation and first-order empirical distinction between packing, aging, and new bottom agglomeration, these two processes would require vertical profiles in the solid fractions and observations of crystal size spectra, which we do not have. Approaches to crystal growth and nucleation on the basis of existing models (e.g. Tsang and Hanley, 1985; Svensson and Omstedt, 1994; Wang and Doering, 2005) would in addition require the vertical distribution of supercooling, in particular near the surface. Without these observations, we cannot distinguish the contributions, neither through empirical means, nor by model validation. Hence, it is important to note that we currently do not know to what degree the determined decay scales depend on the experimental conditions like wave-induced mixing, wave amplitude, ice thickness and heat flux.

However, there are some general results that can be pointed out: First, Fig. 4 shows that in E1 and E3 there is a persistent increase in the bulk frazil thickness H_i over at

TCD
5, 1835–1886, 2011

least 20 h, after which it eventually evens out. This can also be seen in E2 and E4 if the observations are moved forward in time by an offset of 5–10 h, due to the presence of frazil when the experiment started. Therefore, secondary nucleation in the water column, implying thickness increase rather than internal freezing of existing frazil, is always present. An interesting observation is seen during E1 near hour 9, where the thickness rather abruptly increased by ∼1 cm, while the temperature recorded by the CTD instruments increased. This signal, seen in both tanks, is apparently related to the wave paddle stop and may reflect the sudden upward settling of frazil submerged in the water column. From the ∼1 cm thickness increase and a typical solid fraction of 0.1 for the early packing mode in Fig. 6, as well as the depth of the tank below the wave height 85 cm, we can obtain an estimate $(1/85) \times 0.1 \approx 0.0012$ for the suspended frazil volume fraction. Although data are in general sparse, values of a few tenths of a percent have been proposed on the basis of observations in flumes and rivers (Tsang, 1986; Marko and Jasek, 2010). In a similar tank experiment, albeit under the presence of currents rather than waves, Smedsrud (2000, 2001) observed average solid fractions around 0.001. However, in the latter experiments, sediments may have influenced the suspension capability.

Secondly, both the time and thickness fits yield a similar v_{s0} in the range 0.03 to 0.05 at the onset of frazil formation. This corresponds to the first frazil observed at the surface. That this result is not simply due to an inexact timing of the onset of frazil formation is supported by the thickness fits, where it refers to the solid fraction at zero thickness, and by the histogram distribution in Fig. 6, where it also emerges as a peak in the distribution. Intuitively this result may be interpreted in terms of a critical frazil concentration at which crystal interaction becomes too strong to keep the particles in suspension. However, we need to note that these values may also be related to our sampling technique: our first low-porosity ice samples were typically 0.5–1 cm in thickness and it is plausible that a frazil volume fraction of 0.001 exists mixed within the water column; sampling 30 cm of the water column with the cylinder we used would create a volume fraction of 0.03–0.06 if the sampled frazil rises towards the

TCD
5, 1835–1886, 2011

surface and accumulates. A sampling time of 1 min would be sufficiently long to allow for this process. The balance between crystal rise velocity and turbulence production has been pointed out by modellers; e.g., Omstedt and Svensson (1984); Svensson and Omstedt (1994); Wang and Doering (2005). When flocculation becomes large due to crystal interaction, larger crystal ensembles may form and float to the surface. Although this is a very important general aspect, also for proper model simulation and validation (e.g. Omstedt and Svensson, 1984), so far there exist few observations. Osterkamp et al. (1975) estimated, based on conductivity measurements, short-term maximum suspended ice volume fractions of 0.008–0.047 in a subarctic stream, while Tsang (1986) estimated 0.01–0.02. To study how and if the transition depends on the turbulence level, rate of ice formation and crystal shapes, more observations under different growth conditions are needed. Our estimate is a first step and consistent with the crude observations so far.

The maximum solid fraction was obtained here by maximizing the correlation of the exponential fit to the data. Also, the packing law we present is tentative, and assumed as an equation of the type that often describes natural growth and decay processes. Yet, the observations are fitted reasonably well with this approach. The maximum solid fraction as well as the decay time, reflect a combination of packing and crystal growth, and their interaction. The processes are not expected to be additive: e.g., when internal freezing decreases the solid fraction, this may be expected to decrease the mechanical packing rate, whereas settling of new loose crystals will enhance it. As mentioned, we do not intend to speculate on these interactions, on the basis of the present data. However, we can interpret the histogram distribution in Fig. 6 in the following manner. Two prominent peaks in the solid fraction are seen, one in the range 0.09–0.12, the other in the range 0.18–0.26. As the lower peak is only seen in E1 and E3, it appears to be related to the early growth phase. Note that these are the average solid fractions from Eq. (8), while the surface values from Eq. (7) are higher. An early $\overline{v_s} = 0.1$ corresponds to a surface v_s of 0.15, while the second mode gives surface values from 0.25 to 0.28. As the average values are influenced by accumulation of loose frazil from below, we

TCD
5, 1835–1886, 2011

interpret the surface numbers as the packing modes. The second mode is very broad. Such a behaviour appears to be consistent with a first phase dominated by mechanical packing (up to $v_s \approx 0.15$), followed by a second phase where internal crystal growth increases the solid fraction further, as for a constant heat flux the distribution becomes rather constant. Hence, the broadening of the peak towards large v_s is consistent with compaction by internal freezing, while the first is a mechanical compaction mode. This interpretation is also consistent with the observation that above a solid fraction of 0.30 the surface begins to become solid, while up to this limit internal freezing takes place, but the grease still remains a mushy layer and does not freeze up.

To compare the results with other observations, we first emphasise that the distribution in Fig. 6 contains only a few values above 0.30. While internal growth may increase the solid fraction beyond 0.3, in principle limited by 1, such ice would, however, no longer be classified as frazil ice, and consequently only a few (14) high solid fraction samples exist in our data. We note that this interpretation is also consistent with our earlier analysis of the frazil–pancake transition, during the second day of E2 from hour 19 to 43 (De la Rosa et al., 2011), where the frazil ice solid volume fraction, sampled between the pancakes, remained rather constant around 0.27±0.02. Note that the corresponding values shown here in Fig. 5c are slightly different, as we computed them as thickness-weighted solid fractions.

Detailed observations of the solid volume fraction of frazil ice grown in a wave tank have been presented by Martin and Kaufmann (1981). These authors reported solid fractions of 0.18–0.22 from a few centimetres thick grease ice cover, as well as 0.32–0.44 at a distance where the waves had been damped and the ice growth was typically 10 cm. However, as discussed above, the *ice concentrations* reported by them still contained, on average, 11.8 g NaCl kg^{-1}, compared to 38.4 gNaCl kg^{-1} in the water. This implies that the drained crystals still contained considerable liquid. From Eqs. (1) and (2), we obtain a corrected estimate of the true solid fraction by reducing the numbers by an average factor of 0.72. This yields 0.13–0.16 for the young frazil at the leading edge and 0.23–0.32 further "down-wave". The ice volume fraction range of

TCD
5, 1835–1886, 2011

0.35–0.4 reported by Martin et al. (1977) for another laboratory study was determined by the same method and is likely biased by a similar factor. Likewise, computations by Doble et al. (2003) and Doble (2007), who quote a typical solid fraction of 0.4 for frazil slicks in the Weddell Sea, are likely biased by at least a similar factor. Solid volume fractions of 3 to 30 cm thick field grease samples obtained by Smedsrud and Skogseth (2006) do not need to be corrected for the residual ice salinity. However, by comparing their Eq. (5) with our Eq. (2), one can see that theses authors underestimate the solid fraction by typically 10 %. Applying this correction to the field data from Smedsrud and Skogseth (2006), yields solid fractions that fall in the range 0.18 to 0.35, with most observations in the range 0.2 to 0.25. In Maus and De la Rosa (2011) we summarise additional published and unpublished data sources of very young frazil in the range $0.05 < v_s < 0.12$.

In summary, by correcting earlier observations of solid ice volume fractions of grease ice, we obtain values mostly between 0.2 and 0.3 for aged frazil, while youngest frazil observations from previous studies fall in the range 0.05–0.18. Hence, other observations also support the two solid fraction modes we conjectured from this study, indicating a mean of 0.09–0.12 during very early growth and 0.18–0.26 at a later stage.

5.3 Frazil-pancake transition

We can draw on these results by considering the onset of pancake formation, which took place after 17–21 h in E1 and E2 compared to 3–5 h in E3 and E4. In E3 predominantly small pancake-like shuga formed, and E4 thus appears to be the only experiment with early formation of large (∼20 cm) pancakes. However, E4 is different in terms of its much lower wave amplitude (∼1 cm compared to 3–6 cm in other experiments). We thus focus here first on experiments E1 and E2.

The onset of shuga and pancake formation in E1 was observed after approximately 17 h. Comparison with Fig. 11c shows that this is comparable to 3 times the decay timescale $1/c_1 \approx 6$ h for the solid fraction, or the slightly shorter value of 4 h obtained from the critical equivalent thickness scaled by ice growth. In other words, the onset

TCD
5, 1835–1886, 2011

of pancake formation corresponds to a state when $1 - \exp^{-3} \approx 95\,\%$ of the maximum compaction of the frazil has taken place. This result is consistent with the compaction scenario and can be intuitively interpreted as follows. Once frazil ice has reached its maximum mechanically packed state, any further increase in solid fraction due to freezing will imply the freezing of crystals to each other. This state may be indentified with the onset of pancake formation. It appears to take place at a characteristic solid fraction of $0.24 < \nu_{smax} < 0.28$. However, this critical range should be viewed in connection with a statistical distribution of solid fractions: i.e., when it is reached, there are already some locations with higher solid fractions where pancake formation starts. In Fig. 11c there is, after 17 h, an increasing number of solid fractions in the range above 0.3, with a maximum of 0.43. Hence, as already pointed out from Fig. 6 and from the timing of pancake observations and compaction, a solid fraction range 0.3–0.4 appears as the regime where pancakes ultimately start to form locally. Turning back to E4, this view is finally consistent with the early onset of pancake formation in this experiment, where average solid fractions above 0.2 were already present after a few hours (see Fig. 5c and d).

That pancakes generally are thinner than the frazil ice surrounding them (we found a factor of 1/1.5) is consistent with the fact that heat is removed at the surface, and freezing of crystals to each other will be initiated there. Concerning the freezing from the top, we used in our earlier study of the second phase of E2 (De la Rosa et al., 2011) additional infrared surface temperature observations to distinguish between pancake and frazil/grease ice. From this classification we found a transition to pancakes when surface temperatures are 0.7–0.9 K below the freezing point of seawater underneath. Assuming the salinity of the frazil (~25) and a linear temperature gradient in a representative upper layer, we arrived to an estimate of 0.37–0.40 for the solid fraction transition to pancakes. This range is supported from the present analysis of all experiments. While other authors have not explicitly analysed the transition, it is also consistent with highest frazil and grease solid fractions of 0.35 observed in other studies (see above).

TCD
5, 1835–1886, 2011

5.4 Influence of waves

It may be postulated that the frazil ice thickness stops increasing thermodynamically, once a maximum wave height is achieved (w_h times a certain coefficient of change) and the amplitude (or wave height) begins to decrease. The general role of waves in the problem is apparent: they are the source of the turbulence that keeps the frazil ice in suspension. By creating periodical fluid motion, they persistently transport frazil crystals downward and distribute them to a larger depth than if they would accumulate at the surface. Once there is too much ice in the water, and the crystals form large assemblages, the waves are no longer capable of keeping most of the ice in suspension. This appeared to happen quite rapidly, with a grease skim covering the surface after a few hours. However, under the action of waves, it takes much longer time for this grease skim layer to freeze into solid pancakes.

In this scenario the wave amplitude must play an important role. As already mentioned, during E1, with wave amplitudes of 2.8–3.3 cm, this took place after 17 h, while during E4, with amplitude of 1.0–1.2 cm, it appeared after 5 h. Hence, the transition time to pancake formation appears to scale with the amplitude of the waves. However, the agreement is in reality somewhat lower, as E4 started with ~0.4 cm equivalent ice thickness, which implies that the starting time of E4 in terms of ice production onset should be increased by 5 to 10 h (see Fig. 7), giving a corresponding pancake formation time of 10–15 h. Also for E2 such a correction would yield an increase in the pancake formation time to 29–31 h, and in the latter experiment the wave amplitude was indeed largest, initially 4.6–6.0 cm. However, in E2 the wave amplitude was then decreased to 2.6 cm, after which pancake formation set in immediately. Hence, although the evaluation remains qualitative, there is support that the time when pancake formation starts approximately scales with increasing wave amplitude.

Taking the simplest view, that frazil is well mixed on the order of the wave height, however does not consider the feedback that frazil also influences the wave field and amplitude. This was considered in Fig. 9, where both the average wave height and

TCD
5, 1835–1886, 2011

its decay coefficient in the centre of the tank are plotted against the ice thickness normalised by the wave height, $h = H_i / w_h$. Results are most consistent for the attenuation rate, and when the latter is normalised by the different background noise levels in tanks A and B (Fig. 9c). During the first period, wave height is rather constant and wave decay, related to reflections in the tank, is not affected by the increasing ice thickness. When the thickness reaches 0.5–0.6 of the wave height, i.e. a value close to its amplitude, damping increases linearly with thickness. Finally, when the ice thickness reaches 0.7 to 1 times the wave height, the damping becomes very strong and wave height decays considerably. Note that this regime was reached during E1 when the ice thickness reached 4.5–6 cm; from Figs. 3 and 4 it is evident that this occurred after approximately 15 h. Hence, in E1 the onset of strong wave damping coincides closely with the formation of the first pancakes. As another indicator of this transition one notes the change in the slope in the time-thickness plots in Fig. 4 after approximately 15 h.

Wave motion not only stirs the frazil and prevents it from freezing, it also stirs the water. The question from which levels the heat lost through the surface is derived, is important, as it determines the relative contributions of secondary nucleation and crystal growth within the surface grease. An interesting event in this context was the wave paddle stop that took place from hour 9–11 in E1. This corresponded to an increase of 0.03 K in the temperatures recorded at all four CTD instruments (Fig. 2b, c), at 40 and 65 cm depth of the 85 cm deep tank. This warming rate, if it occurred over the whole tank, corresponds to a heat flux of 15 Wm^{-2}. We interpret this as the heat that the tank receives through its bottom and side walls, suggesting that the heat fluxes given in Fig. 8 are net heat fluxes, whereas the surface forcing is likely larger by this amount. Note also that the temperature, after restarting the wave paddle, returns to its original value after just half an hour, corresponding to a net heat loss of 60 Wm^{-2}, which is the value derived for this experiment. Hence, wave motion appears, at least in E1, effective enough to distribute the heat loss over the whole water column.

Wave damping, once it sets in, may thus have a two-fold effect. First, it no longer stirs the frazil crystals in the grease ice layer, leading to compaction. Second, it implies

TCD
5, 1835–1886, 2011

that the heat released to the atmosphere (withdrawn by the roof cooling aggregate) derives from a thinner water layer and grease. Both processes are favourable for an increased solid fraction and the onset of pancake formation. Another aspect to discuss in this context is the normalised ice thickness to which the frazil may grow after the onset of strong wave damping. The histogram in Fig. 10 shows that for E1–E3, for which conditions in terms of amplitude and heat flux were very similar, this limit was approximately 1.5 times the wave height. However, in E2 the wave amplitude was decreased after 19 h, and the evolution was thus not continuous. On the other hand, for E4 wave heights were small and the grease ice thickness reached 3 times the wave height by the end of the experiment. For comparison, we obtained from Table 1 in Martin and Kauffmann (1981), an average of $H_i/w_h = 2.3 \pm 0.7$ for the location within the grease ice where the amplitude had decayed to typically 1/4 of its initial value (noted as "dead zone" by the authors). It thus appears that frazil may accumulate to 2–3 times the wave height, even when the waves are strongly damped, and that most experiments were too short to reach this limit. For example, in tank experiments reported by Leonard et al. (1999) H_i/w_h appears to have reached values slightly above 1 (their Figs. 3 to 7), but their observations span less than 20 h. Clearly, more observations under varying heat flux and wave conditions are needed to better constrain such a bound.

5.5 Heat fluxes

Heat flux in each tank is evaluated from Eq. (1) based on observed cooling rates, prior to freezing, and from the change in ice bulk mass during the runs. The latter method yields less accuracy, due to an inhomogeneous wave field, advection along the tank, and observational uncertainties of solid fraction. Unfortunately, no observations of solid ice growth were obtained in the quiet tank for calibration. However, for E1 the spatial and temporal resolution was sufficient to derive the net heat flux with 10 % accuracy. In general the results suggest that the heat loss from the surface is not kept constant by the cooling aggregate. The observations with high significance are consistent with a heat flux that is proportional to the temperature difference between the

TCD
5, 1835–1886, 2011

ice/water surface and a fixed level above, $Q = k_a(T_a - T_s) - Q_0$. As mentioned, the heat flux Q_0 that presumably takes place through the tank wall and bottom, was estimated as roughly 20 % of the amount entering at the surface. It is of interest to know whether the changes in the room temperature are induced by surface changes or vice versa, and to what degree the response in the closed room laboratory is similar to that in a free atmosphere. To study the likely heat flux reduction induced by a colder pancake ice cover, surface temperature data would be needed for all the experiments. In the present study these were available only for the second phase of E2. Hence, from the present data, and also insufficient records on the cooling aggregate power applied, the response cannot be determined quantitatively.

The heat fluxes through the tank surface and walls very likely influence the frazil ice formation within the water column and may do so in a different manner for different wave amplitudes. For instance, one may consider ice growth with $d(H_i v_s)/dt = Q/(L_f \rho_s)$and assume that H_i becomes constant or changes little due to a wave imposed limit. In this situation the rate in solid fraction increase dv_s/dt will become proportional to the heat flux, if the heat is removed from the grease ice layer alone. However, due to wave-induced mixing, only a fraction of heat is released by freezing near the surface - the remaining heat comes from nucleation of crystals within the water column, and from the heat input through the tank walls. To evaluate mechanical compaction and internal freezing of grease ice, observations of temperature and crystal size distribution in the water column, as well as in the grease ice itself would be necessary.

5.6 Grease ice temperature

The findings discussed above show that profiles of solid fraction would improve our understanding of the packing and consolidation process of grease ice. The same is true for the salinity and temperature of the liquid fraction of grease. In the present work we have assumed that due to wave-stirring, the brine has the properties of the seawater on which the grease floats, with the temperature given by the freezing point of seawater. However, this assumption is due to a lack of observations as we unfortunately, did not

TCD
5, 1835–1886, 2011

measure the salinity of the brine. Information from other investigators is sparse, but some does exist. Martin (1977) shows a temperature profile in 6 cm thick grease ice grown in a wave field and an air temperature of −18.8 °C: a submerged probe showed a 0.1 K lower temperature only at the surface, while the rest of the ice had temperatures within 0.01 K of the seawater below. Surface measurements with a submerged probe performed by S. Maus (unpublished data) also gave 0.1 K lower temperature than the seawater below. Ushio and Wakatsuchi (1993) report, in a laboratory experiment of frazil ice formation, a 0.04–0.07 K warmer grease layer compared to the water below. However, because the water was supercooled by 0.1–0.2 K, this suggests that the grease had temperatures 0.06–0.13 below the freezing point of the underlying water. From the IR surface temperature observations of the second phase of E2, when pancake formation had started, De la Rosa et al. (2011) found a characteristic surface temperature of frazil that was 0.47 K lower than the seawater below. However, this signal could be restricted to the very surface skim (Katsaros, 1973). The thermistor data from that study indicated that the frazil temperature was not more than 0.1 K below the temperature of the water, but the accuracy was too low to derive any significant difference.

6 Conclusions

In the present study we have analyzed the growth of frazil ice under the presence of waves. Our main focus was to describe the evolution of its salinity and solid fraction during its accumulation in a floating grease ice layer, until its transition into solid pancakes. Derived solid fractions and salinity refer to frazil ice in situ, rather than sieved frazil crystals, and we emphasize to use this approach, presented in more detail in a follow-up paper (Maus and De la Rosa, 2011), to describe frazil properties.

Frazil ice growth and accumulation in our experiments proceeded, in accordance to earlier studies, as follows: A water column, mixed by wave-generated turbulence, was

TCD
5, 1835–1886, 2011

cooled to – and likely supercooled some hundredths of a degree below – the freezing point. Growth of frazil crystals then started and released latent heat, decreasing the supercooling. Ice growth then proceeded, without major changes in the temperature, driven by the heat loss from the tank. After a few hours, a surface grease ice skim of low porosity and a few millimetres in thickness was observed. It increased subsequently growing in thickness and solid fraction until, after slightly less than a day, the first pancakes appeared. Based on our observations we identified these regimes with the following transitions in terms of the solid fraction and thickness:

(1) The first grease ice that appears at the surface (interpolating the results to zero thickness), has a solid fraction of 0.03–0.04. Although we think that this value likely relates to sampling of the water column, for which frazil with a volume fraction of typically 0.001 was estimated, it indicates the lowest packing that frazil may obtain. It further points to the important question, at which particles in a frazil suspension begin to interact rigorously to from clusters that float to the surface.

(2) A histogram of all solid fractions obtained shows a major solid fraction peak in the range 0.18–0.26, with almost no frazil having solid fractions above the latter value, yielding a tentative upper limit for the solid fraction of frazil.

(3) The solid fraction evolution can be approximated by an exponential compaction law, with a maximum solid fraction of 0.23–0.28. In terms of a decay time scale, it takes 12–18 h until 95 % of the frazil compaction to its maximum solid ice fraction is reached.

(4) The decay time scale coincides with the onset of pancake formation.

(5) Strong wave damping is first observed when the ice thickness reaches 0.7–0.9 times the wave height. This transition corresponds to the 95 % decay time of the solid fraction and the onset of pancake transition as well.

TCD
5, 1835–1886, 2011

From these findings we conjecture that there is a critical solid fraction of dense frazil ice suspensions, above which any further increase will lead to the formation of a solid ice matrix, i.e., pancake ice. This transition appears to depend on wave action. Once waves are strongly damped, the grease is no longer stirred, latent heat is released preferentially from crystals close to the surface and freezing into solid pancakes begins. While the details of how grease porosity, heat transport and waves interact to delay and initiate freeze-up still remain challenging, the present dataset and analysis provides some parameter estimates and hypothesis to guide future modelling of grease and frazil ice. First, basic models of nucleation and surface skim formation (e.g., Omstedt and Svensson, 1984) may be further developed and validated including a time-dependent solid fraction, as well as the critical concentration at which frazil crystals tend to accumulate at the surface. Second, the opening and closing timescale of leads and polynyas is strongly related to the ratio $(L_f \rho_i H_i v_s)/Q$, wherein both ice thickness H_i and solid fraction v_s appear (e.g., Bauer and Martin, 1983; Pease, 1987; Biggs et al., 2004). So far the solid fraction has been treated as constant in most models. The present study suggests decay timescales for the solid fraction of more than half a day, indicating that its treatment in many model applications may be important. The results of this study can be relevant to device the transition from a grease to pancake ice cover on the basis of thermodynamic constraints. Such approaches may improve presently incomplete theories of grease ice viscosity and wave damping (e.g., de Carolis, 2005; Wang and Shen, 2010a, b). Finally, we would like to note that the importance of freezing processes in turbulent seawater may increase in the future, given the transformation of the Arctic sea ice cover. Decreases in the sea ice extent in summer have been – and are predicted to be – relatively large compared to the winter (e.g., Serreze et al., 2007). Frazil ice growth may thus become more common in the near future, expanding the seasonal ice zone area with implications for upper layer oceanography and thermodynamics.

TCD
5, 1835–1886, 2011

Acknowledgements. This work describes the RECARO project (Principal Investigator: Jeremy Wilkinson from the Scottish Association for Marine Science) supported by the European Community's Sixth Framework Programme through the grant to the budget of the Integrated Infrastructure Initiative HYDRALAB III, Contract no. 022441(RII3). The work was completed as part of the NorClim project, funded by the Norwegian Research council. We thank the Hamburg Ship Model Basin (HSVA, www.hsva.de), especially the ice tank crew, for the hospitality, technical and scientific support and the professional execution of the test program in the Research Infrastructure ARCTECLAB. Ruixue Wang (Uni. Manitoba, Canada) is thanked for providing the wave data and for valuable discussions, Lars H. Smedsrud (Uni. Bergen, Norway) for providing the sampling cylinder, Hayley Shen (Potsdam, USA) and Shigeki Sakai (Uni. Iwate, Japan) are thanked for providing pancake observations and Marcel Nicolaus (AWI, Germany) for the thermistor data. Peter Haugan, Martin Miles (Uni. Bergen, Norway) and Laurent Bertino (NERSC, Norway) are acknowledged for pre-submission reviews of text. The first author finally thanks Trond Mohn c/o Frank Mohn AS for providing partial funds for this work.

References

Carstens, T. J.: Experiments with supercooling and ice formation in flowing water, Geofys. Publ. Norway, 26 (9), 3–18, 1966.

Clark, S. P. and Doering, J. C.: Frazil flocculation and secondary nucleation in a counter-rotating flume, Cold Reg. Sci. Technol., 55 (2), 221–229, 2009.

De la Rosa, S., Maus, S., and Kern, S.: Thermodynamic investigation of an evolving grease to pancake ice cover, Ann. Glaciol., 52 (57), 206–214, 2011.

De Carolis, G., Olla, P., and Pignagnoli, L.: Effective viscosity of grease ice in linearized gravity waves, Fluid Mech. 535, 369–381, 2005.

Doble, M.: Growth and motion at the Weddell Sea-ice edge, University of Southampton, Faculty of Engineering Sciences and Mathematics, School of Ocean and Earth Sciences, Doctoral Thesis, 170 pp., (http://eprints.soton.ac.uk/63134/1.hasCoversheetVersion/Doble_2007_PhD.pdf), 2007.

Katsaros, K. B.: Supercooling at the surface of an Arctic lead, J. Phys. Oceanogr., 3 (4), 482–485, 1973.

TCD

5, 1835–1886, 2011

Kinnard, C., Zdanowicz, C. M., Koerner, R. M., and Fisher, D. A.: A changing Arctic seasonal ice zone: Observations from 1870–2003 and possible oceanographic consequences, Geophys. Res. Lett., 35, L02507, doi:10.1029/2007GL032507, 2008.

Leonard, G. H., Shen, H. H., and Ackley, S. F.: Dynamic growth of a pancake ice cover, Ice in surface waters: Proceedings of the 14th International IAHR Ice Symposium, Taylor & Francis, Shen (ed.), Rotterdam, ISBN: 90/5410/9718, 1998.

Marko, J. R. and Jasek, M.: Frazil monitoring by multi-frequency Shallow Water Ice Profiling Sonar (SWIPS): present status, Proceedings of 20th International Symposium on Ice, Lahti, Finland, 12 pp., 2010.

Martin, S., Kauffman, P., and Welander, P. E.: A laboratory study of the dispersion of crude oil within sea ice grown in a wave field, Proceedings of the Twenty-Seventh Alaska Science Conference vol. II, American Association for the Advancement of Science, Fairbanks, AK, 261–287, 1977.

Martin, S.: Frazil ice in rivers and ocean, Ann. Rev. Fluid Mech., 13, 379–397, 1981.

Martin, S. and Kaufman, P.: A field and laboratory study of wave damping by grease ice, J. Glaciol., 27 (96), 283–313, 1981.

Maykut, G. A. and Untersteiner, N.: Some results from a time-dependent thermodynamic model of sea ice, J. Geophys. Res., 76, 1550–1575, 1971.

Maus, S.: On Brine Entrapment in Sea Ice: Morphological stability, microstructure and convection, Logos Verlag Berlin GmbH, ISBN: 978-3-8325-1523-2, 538 pp., 2007.

Maus, S. and De la Rosa, S.: Salinity and volume fraction of grease and frazil ice, J. Glaciol., in review, 2011.

Newyear, K. and Martin, S.: A comparison of theory and laboratory measurements of wave propagation and attenuation in grease ice, J. Geophys. Res., 102, 25091–25099, 1997.

Omstedt, A. and Svensson, U.: Modelling supercooling and ice formation in a turbulent Ekman layer, J. Geophys. Res., 89, C1, 735–744, 1984.

Osterkamp, T. E., Gilfilian, R. E., Gosink, J. P., and Bensen, C. S.: Water temperature measurements in turbulent streams during periods of frazil-ice formation, Annals of Glaciology, Internat. Glaciological Society, Proc. Second Symposium on Applied Glaciology, 4, 209–215, 1983.

Reimnitz, E., Clayton, J. R., Kempema, E. W., Payne, J. R., and Weber, W. S.,: Interaction of rising frazil with suspended particles: tank experiments with applications to nature, Cold Reg. Sci. Technol., 21, 117–135, 1993.

TCD
5, 1835–1886, 2011

Serreze, M. C., Holland, M. M., and Stroeve, J.: Perspectives on the Arctic's shrinking sea-ice cover, Science, 315, 1533–1536, 2007.
Shen, H. H., Ackley, S. F., and Yuan, Y.: Limiting diameter of pancake ice, J. Geophys. Res., 109, C12035, doi:1029/2003JC002123, 2004.
Smedsrud, L. H.: Incorporation of sediments into sea ice in coastal polynyas in the Kara sea, Report, Norwegian Polar Institute, Tromsø, Norway, 2000.
Smedsrud, L. H.: Frazil ice entrainment of sediment: large tank laboratory experiments, J. Glaciol., 47 (158), 461–471, 2001.
Smedsrud, L. H. and Skogseth, R.: Field measurements of Arctic grease ice properties and processes, Cold Regions Science and Technology 44 (3), 171–183, doi:10.1016/j.coldregions.2005.11.002, 2006.
Svensson, U. and Omstedt, A.: Simulation of super cooling and size distribution in frazil ice dynamics, Cold Regions Science Technol., 22, 221–233, 1994.
Tsang, G.: Preliminary report on field study at Lachine Rapids on cooling of river and river and formation of frazil and anchor ice. Proceedings of the 4th Workshop on Hydraulics of River Ice, Montreal, F5.1-5.51, 1986.
Tsang, G. and Hanley, O'D. T.: Frazil formation in water of different salinities and supercoolings, J. Glaciol., 31, 108, 74–85, 1985.
Ushio, S. and Wakatsuchi. M.: A laboratory study on supercooling and frazil ice production processes in winter coastal polynyas, J. Geophys. Res., 98(C11), 20321–20328, 1993.
Wadhams, P., Squire, V. A., Goodman, D. J., Cowan, A. M., and Moore, S. C.: The attenuation rates of ocean waves in the marginal ice zone, J. Geophys. Res., 93 (C6), 6799–6818, 1988.
Wadhams, P. and Wilkinson, J. P.: The physical properties of sea ice in the Odden ice tongue, Deep-Sea Res. Pt. II, 46, 1275–1300, 1999.
Wang, S. M. and Doering, J. C.: Numerical simulation of supercooling process and frazil ice evolution, ASCE J. Hydraul. Eng. 131, 889–897, 2005.
Wang, R., Shen, H. H. and Evers, K.-U.: An experimental study of wave induced ice production, 19th IAHR International Symposium on ice, Vancouver, British Columbia, Canada, 2008.
Wang, R. and Shen, H. H.: Experimental study of surface wave propagating through a grease–pancake ice mixture, Cold Reg. Sci. Technol., 61(2–3), 90–96, 2010a.
Wang, R. and Shen, H. H.: Gravity waves propagating into an ice-covered ocean: A viscoelastic model, J. Geophys. Res., 115, C06024, doi:10.1029/2009JC005591, 2010b.

TCD
5, 1835–1886, 2011

Weeks, W. F. and Ackley, S. F.: The growth, structure, and properties of sea ice, in: Untersteiner, N. (Ed.), The Geophysics of Sea Ice. Plenum, New York, 9–164, 1986.
Wilkinson, J.: Sea ice, convection and the Greenland Sea, University of Southampton, Faculty of Engineering Science and Mathematics, School of Ocean and Earth Science, Doctoral Thesis, 234 pp., 2005.
Wilkinson, J. P., DeCarolis, G., Ehlert, I., Evers, K.-U., Gerland, S., Hughes, N., Jochmann, P., Kern, S., Nicolaus, M., Notz, D., De la Rosa, S., Sakai, S., Shen, H., Smedsrud, L. H., and Wadhams, P.: Ice tank experiments highlight changes in sea ice types, EOS Trans. AGU, 10, 81–82, doi:10.1029/2009EO100002, 2009.

TCD
5, 1835–1886, 2011

Table 1. $\overline{T_a}$: mean air temperature from +8 cm above calm water tank and roof (where available). $\overline{T_f}$: mean NaCl solution freezing temperature from top CTD (where available). ΔT_w and ΔS_w: change in water temperature and water salinity during experiment duration. S_{wo}: initial salinity before ice freezing, measured for E1 and E2 from top CTD data, calculated for E4 (see Sect. 3.5) and estimated for E3 assuming same conditions as in E1. H_i, S_i and v_s: maxima and minima values for frazil ice thickness, salinity and volume fraction data. $STD_{\overline{Hi}}$, $STD_{\overline{Si}}$ and $STD_{\overline{vs}}$ denote the average variation of variables H_i, S_i and v_s along the tank and are computed as the mean of the standard variations of each sample set in time. f: wave frequencies applied to each tank. A_0: incoming amplitude measured at sensor group 1 near wave paddle. λ: average wavelength at sensor group 1.

Experiment properties									
	Units	E1 A	E1 B	E2 A	E2 B	E3 A	E3 B	E4 A	E4 B
Total Duration	(h)	51.7	51.7	44.3	44.3	55.4	55.4	46.4	46.4
Start of Pancake ice	(h)	17	17	21	19	3 to 4	3 to 4	5	5
$\overline{T}_a$	(°C)	−9.09 (+8 cm) −10.80 (roof)		−8.72 (+8 cm) −10.55 (roof)		−9.16 (+8 cm)		−12.10 (+8 cm)	
$\overline{T}_f$	(°C)	−2.02	−1.99	−1.97	−1.99	no data	no data	no data	−2.14
ΔT_w	(°C)	−0.14	−0.19	−0.37	−0.09	no data	no data	no data	−0.16
ΔS_w	(g kg^{-1})	1.42	1.78	4.10	1.23	no data	no data	no data	0.71
Sw_o	(g kg^{-1})	33.00	33.17	31.33	33.08	33.00	33.00	35.38	35.38
Frazil ice properties									
H_i min to max $STD_{\overline{H_i}}$	(cm)	0.4–12.0 ±2.3	0.2–9.4 ±2.2	2.5–11.0 ±2.8	0.5–13.5 ±3.1	0.3–11.1 ±2.9	0.3–12.5 ±2.9	1.5–6.0 ±1.7	2.5–6.5 ±1.8
number of samples		117	119	56	55	75	75	42	49
S_i max to min $STD_{\overline{S_i}}$	(g kg^{-1})	31.8–22.9 ±1.05	32.3–20.3 ±1.37	29.7–22.1 ±2.02	31.4–20.6 ±2.96	31.9–24.2 ±1.88	31.1–24.7 ±1.47	30.3–24.2 ±1.02	31.7–25.5 ±1.22
v_s min to max $STD_{\overline{v_s}}$		0.04–0.35 ±0.04	0.03–0.43 ±0.05	0.15–0.36 ±0.06	0.06–0.41 ±0.09	0.04–0.29 ±0.06	0.06–0.27 ±0.05	0.16–0.34 ±0.03	0.12–0.30 ±0.04
number of samples		41	44	19	11	27	31	16	20
Wave properties									
f	(Hz)	0.8984	0.8984	0.6641	0.7813	0.9180 0.8984 0.6641	0.9180 0.8984 0.6641	variable 0.5 to 1.11; 0.70	variable 0.5 to 1.11; 0.72
A_0	(cm)	2.84	3.28	4.61	5.95	3.299 3.778 2.368	3.507 3.630 1.949	1.16	0.98
λ	(m)	1.92	1.92	3.28	2.49	1.84; 1.92; 3.28	1.84; 1.92; 3.28	4.95 to 1.27; 3.01	4.95 to 1.27; 3.01

TCD
5, 1835–1886, 2011

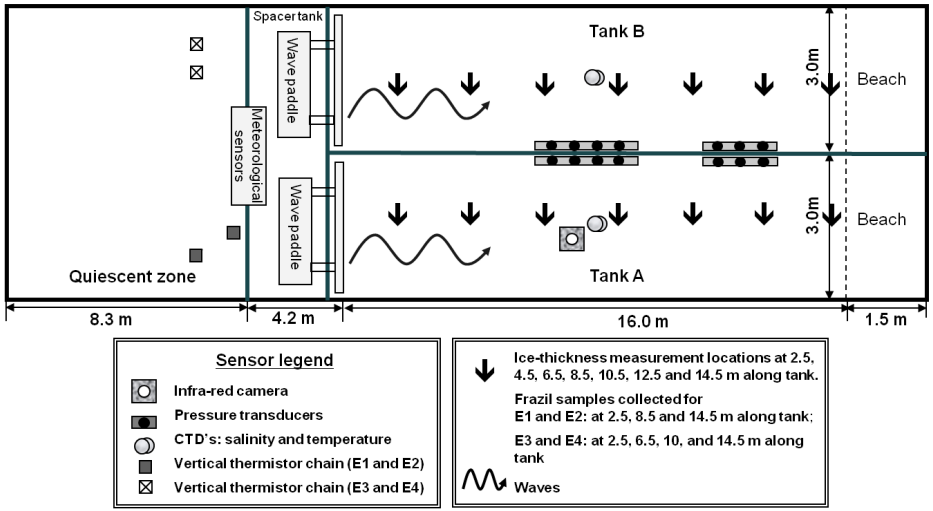

Fig. 1. Top view schema of the laboratory layout (not to scale), modified from Wilkinson et al. (2009) to correct scales and display instruments relevant to this paper.

TCD
5, 1835–1886, 2011

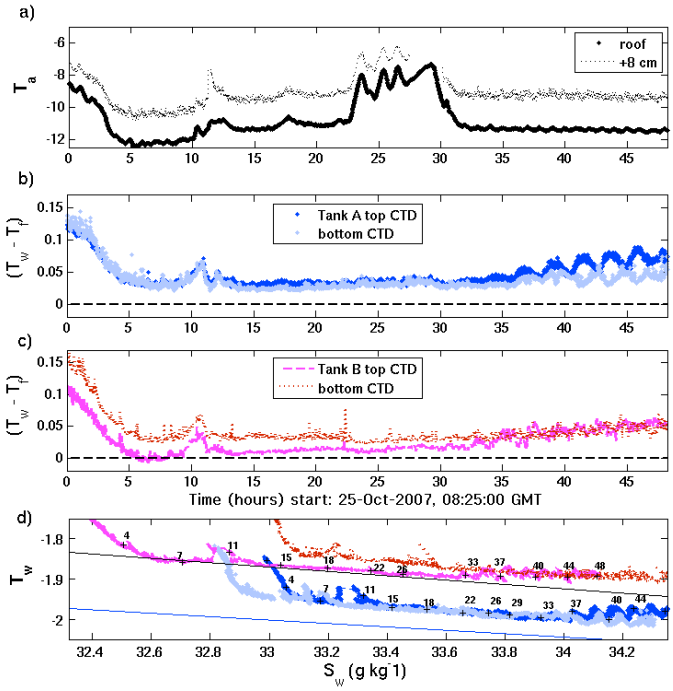

Fig. 2. Air temperatures and CTD data for E1. **(a)** T_a from +8 cm thermistor in quiet tank and roof sensor, **(b)** and **(c)** deviation from freezing temperature for both CTD sensors in tanks A and B, respectively, **(d)** water temperature against salinity for both sensors and tanks. Tank B temperatures (red and pink) are displaced by +0.1 to avoid overlap with tank A data. Constant lines in **(d)** are the water freezing temperature (black line is displaced +0.1, to be comparable with tank B curves). Labeled numbers represent time, for top CTD data in each tank. All temperatures are given in ˚C. X-axis for **(a)**, **(b)** and **(c)** represents time. Legends in **(b)** and **(c)** also apply to **(d)**.

TCD
5, 1835–1886, 2011

Laboratory study of frazil ice accumulation

S. De la Rosa and S. Maus

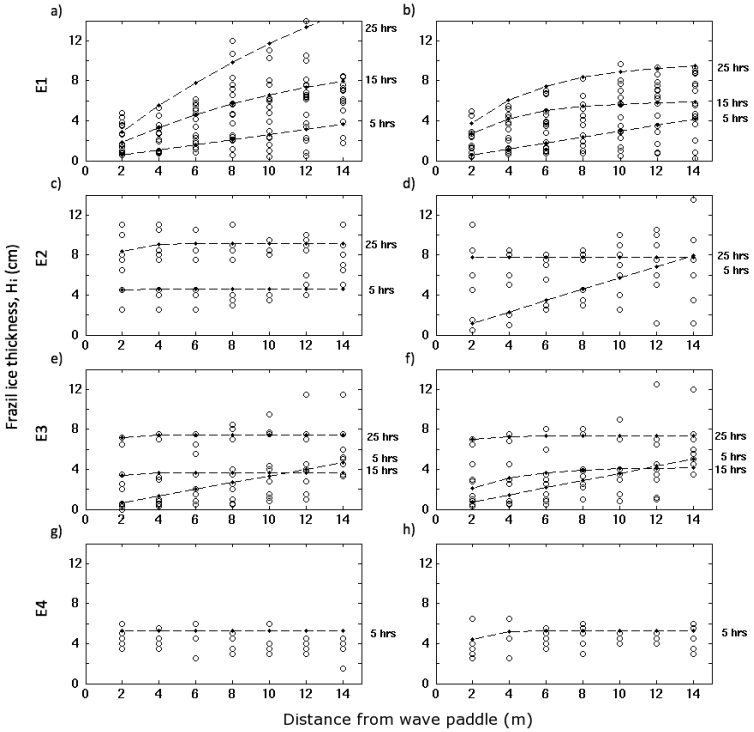

Fig. 3. Frazil ice thickness evolution in along tank for all experiments: **(a)** and **(b)** E1, **(c)** and **(d)** E2, **(e)** and **(f)** E3, **(g)** and **(h)** E4. Panels to the left display data from tank A, panels to the right display data from tank B. The dashed lines correspond to mean ice thicknesses (for 5, 15 and 25 h where available) from an exponential growth model, H_{im}. See Sect. 3.3 for description of H_{im} calculation.

TCD
5, 1835–1886, 2011

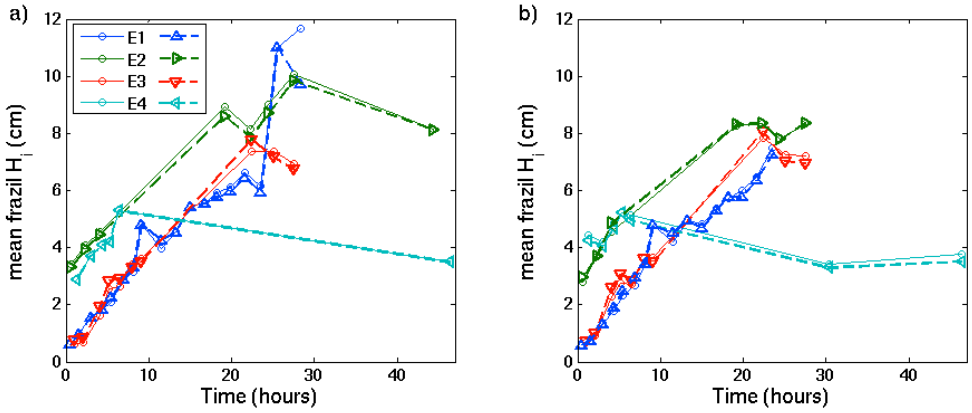

Fig. 4. Comparison for each experiment of mean observed $\overline{H}_{\mathrm{i}}$(thin solid lines) and mean exponentially fitted thickness $\overline{H}_{\mathrm{im}}$ (thick dashed lines). Panel **(a)** corresponds to tank A, panel **(b)** to tank B.

TCD
5, 1835–1886, 2011

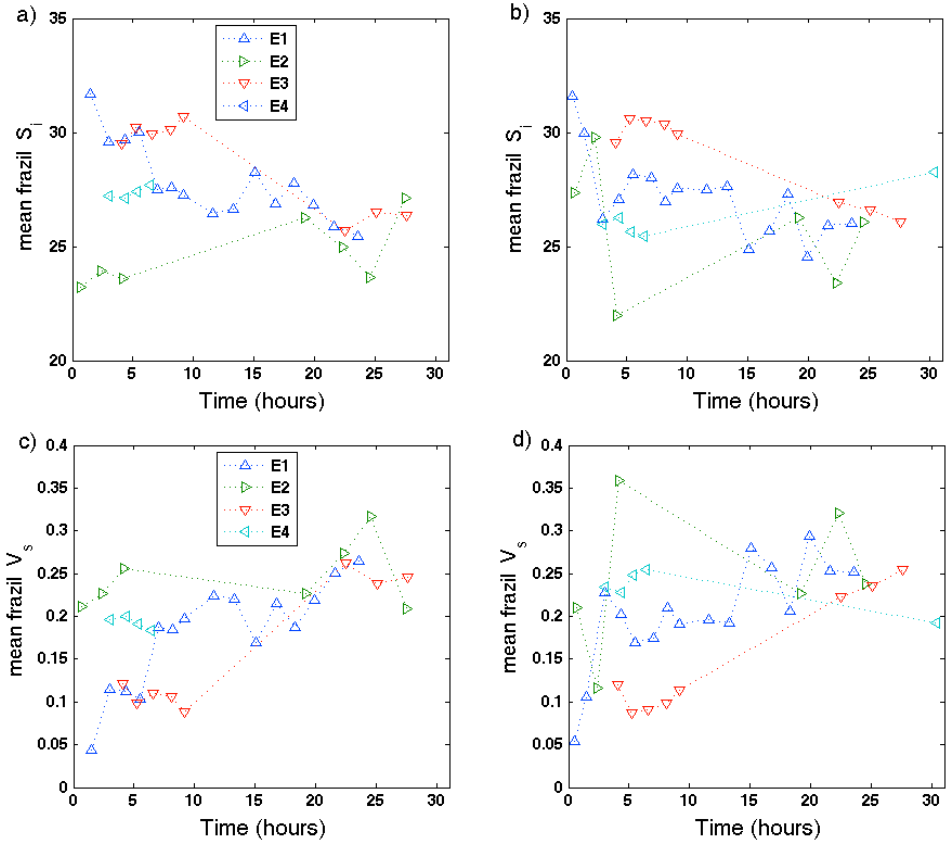

Fig. 5. Time evolution of the thickness-weighted mean frazil ice salinity (Eq. 5) for all experiments **(a)** tank A, **(b)** tank B and mean frazil ice volume fraction tank A, **(d)** tank B.

TCD
5, 1835–1886, 2011

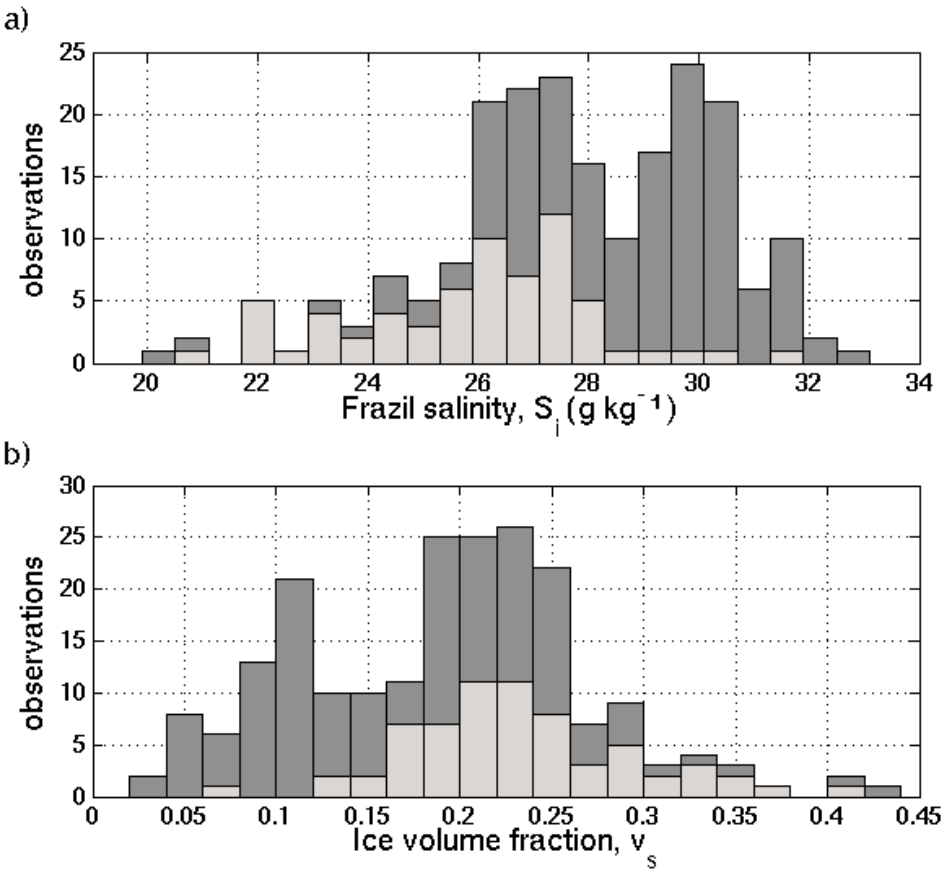

Fig. 6. Histograms for all experiment observations for **(a)** ice salinity centred in 0.6 g kg^{-1} bins and **(b)** frazil ice solid fraction, centred in 0.02 bins. Light gray distributions show data from E2 and E4 only.

TCD
5, 1835–1886, 2011

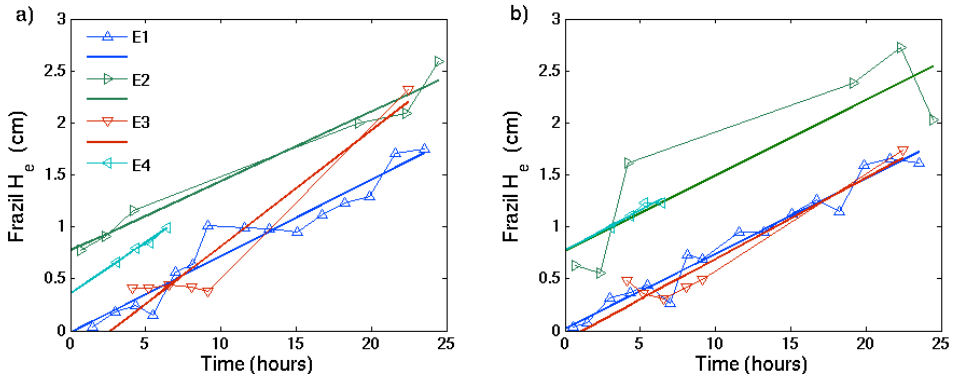

Fig. 7. Mean equivalent ice thickness $\overline{H_e}$ during frazil ice growth (thin solid lines) and corresponding predicted growth line from estimated Q_t (thick solid lines). Panel **(a)** corresponds to tank A, panel **(b)** to tank B.

TCD
5, 1835–1886, 2011

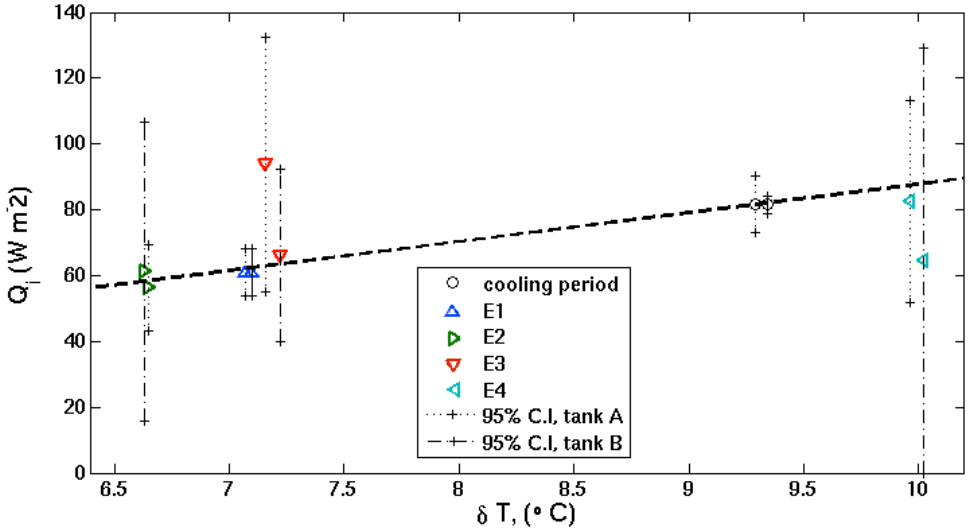

Fig. 8. Variation of derived Q_s and Q_i with mean temperature difference between water and air for each experiment and tank. Upper and lower (95 % confidence interval) limits are given with vertical black lines: tank A (dotted) and tank B (dash dot). Tank B points for the cooling period, E3 and E4, have been displaced in the x-axis by +0.06 units, for visibility.

TCD
5, 1835–1886, 2011

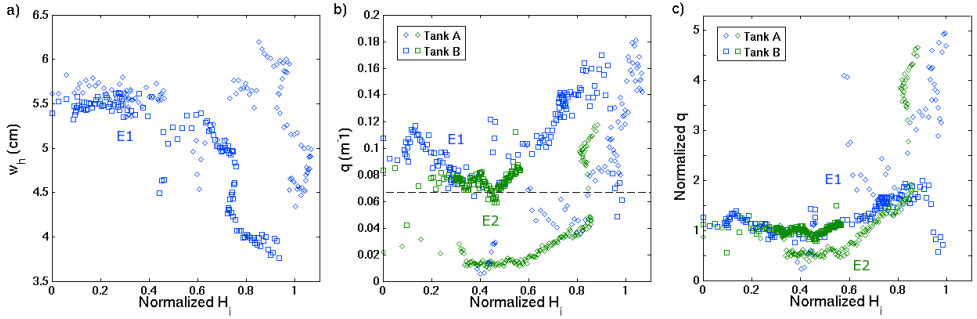

Fig. 9. Scatter plot of **(a)** wave height **(b)** attenuation rate and **(c)** normalized attenuation rate against the mean normalized ice thickness for each tank data. **(a)** shows data for E1 only **(b)** and **(c)** show data for E1 and E2. Wave height and ice thickness data from both sensor groups were meaned before plotting. The dashed black horizontal line in **(b)** is the e-folding scale of the tank (1/L).

TCD
5, 1835–1886, 2011

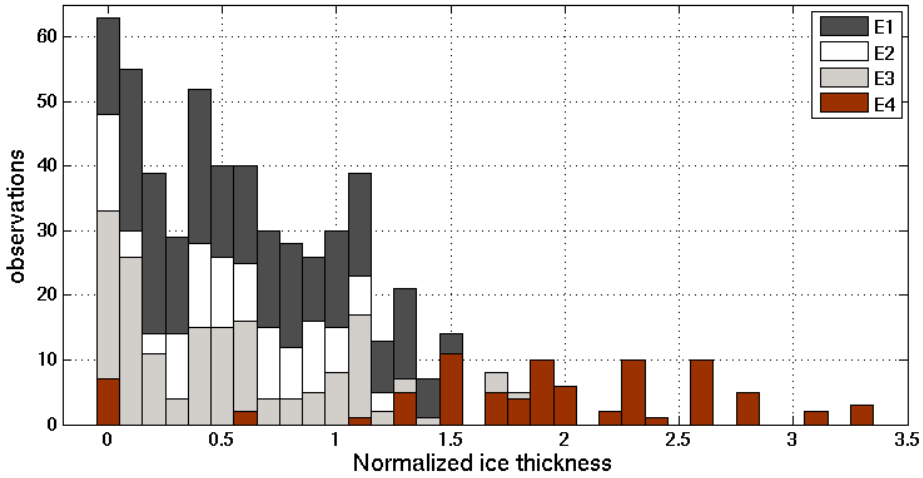

Fig. 10. Histogram of ice thickness normalized against initial wave height for all data. Data for E1 in dark grey, E2 in white, E3 in light gray and E4 in brown. Bins set at 0.1.

TCD
5, 1835–1886, 2011

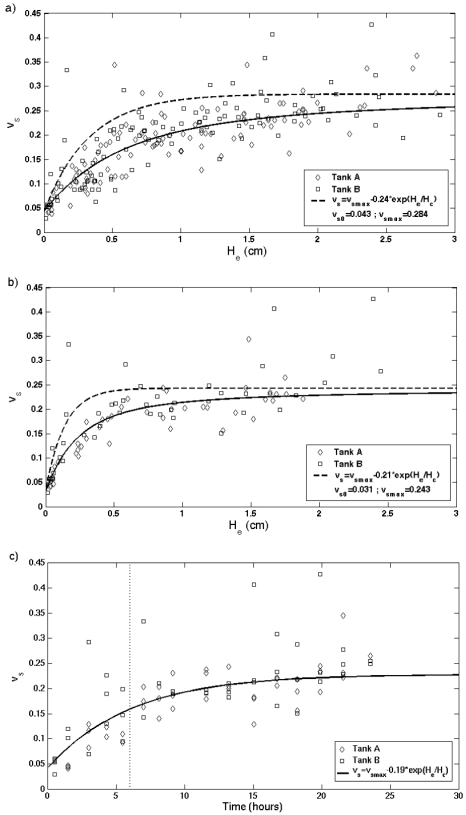

Fig. 11. Frazil volume fraction v_s against equivalent frazil ice thickness H_e, tank A (squares) and tank B (diamonds) **(a)** for all experiment observations and **(b)** for E1. **(c)** v_s for E1 against time, limited to 30 h growth. A mean exponential relation (solid curve) is applied in each case through all the data points integrated with depth and in **(a)** and **(b)** also a maximum exponential relation (dashed curve) is included, representing compacted frazil at the surface.

TCD
5, 1835–1886, 2011